Journal of Colloid and Interface Science 504 (2017) 457–467

Contents lists available at ScienceDirect

Journal of Colloid and Interface Science

journal homepage: www.elsevier.com/locate/jcis

Regular Article

Mechanisms of soil humic acid adsorption onto montmorillonite and kaolinite

Hongfeng Chen [a], Luuk K. Koopal [a,b], Juan Xiong [a], Marcelo Avena [d], Wenfeng Tan [a,c,*]

[a] Key Laboratory of Arable Land Conservation (Middle and Lower Reaches of Yangtze River), Ministry of Agriculture, College of Resources and Environment, Huazhong Agricultural University, Wuhan 430070, PR China
[b] Physical Chemistry and Soft Matter, Wageningen University and Research, Stippeneng 4 (Helix), 6708 WE Wageningen, The Netherlands
[c] State Key Laboratory of Soil Erosion and Dryland Farming on the Loess Plateau, Institute of Soil and Water Conservation, Chinese Academy of Sciences and the Ministry of Water Resources, Yangling, Shaanxi Province 712100, PR China
[d] INQUISUR, Departamento de Química, Universidad Nacional del Sur (UNS)-CONICET, Av. Alem 1253, B8000CPB Bahía Blanca, Argentina

GRAPHICAL ABSTRACT

The thermograms (exothermic) of the stepwise of adsorption of JGHA on kaolinite (KAO) and a schematic indication of JGHA adsorption on the edge and basal faces of KAO at pH 4.0 and 8.0. The sites on edge face ascribed to the high molar enthalpy adsorption sites and the O and T basal face ascribed to low molar enthalpy adsorption sites. The different colours of JGHA molecules represent JGHA adsorption on the face of KAO driving by different mechanisms.

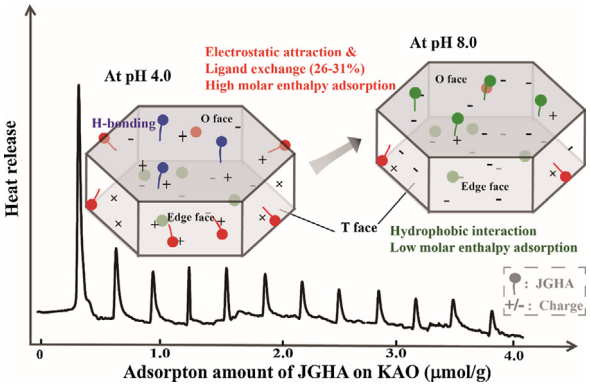

ARTICLE INFO

Article history:
Received 20 January 2017
Revised 20 May 2017
Accepted 23 May 2017
Available online 24 May 2017

Keywords:
Humic acid
Kaolinite
Montmorillonite
Adsorption isotherm

ABSTRACT

To explore the adsorption mechanisms of a soil humic acid (HA) on purified kaolinite and montmorillonite, a combination of adsorption measurements, attenuated total reflectance Fourier transform infrared (ATR-FTIR) spectroscopy and isothermal titration calorimetry (ITC) was employed at pH 4.0, 6.0 and 8.0. The adsorption affinities and plateaus of HA on the two clays increased with decreasing pH, indicating the importance of electrostatic interaction. The effects were more significant for kaolinite than for montmorillonite. The substantial adsorption at pH 8.0 indicated hydrophobic interaction and/or H-bonding also played a role. The ATR-FTIR results at pH 8.0 showed that the Si-O groups located at basal faces of the two clays were involved in the adsorption process. For kaolinite, at pH 4.0 and 6.0, HA adsorption occurred via OH groups on the edge faces and basal octahedral faces (both positively charged), plus some adsorption at Si-O group. The exothermic molar adsorption enthalpy decreased relatively

* Corresponding author at: Key Laboratory of Arable Land Conservation (Middle and Lower Reaches of Yangtze River), Ministry of Agriculture, College of Resources and Environment, Huazhong Agricultural University, Wuhan 430070, PR China.
E-mail address: wenfeng.tan@hotmail.com (W. Tan).

http://dx.doi.org/10.1016/j.jcis.2017.05.078

Attenuated total reflectance Fourier transform infrared (ATR FTIR)
Isothermal titration calorimetry (ITC)
Clay edge
Clay basal plate
Molar Gibbs energy/enthalpy/entropy of adsorption

dramatically with adsorption up to adsorption values of 0.7 μmol/g on montmorillonite and 1.0 μmol/g on kaolinite, but the decrease was attenuated at higher adsorption. The high exothermic molar enthalpy of HA binding to the clays was ascribed to ligand exchange and electrostatic binding, which are enthalpy-driven. At high adsorption values, JGHA adsorption by hydrophobic attraction and H-bonding also occurs.

1. Introduction

Humic acid (HA) is an important component of humic substances, which are dominant organic components in soils, sediments and aquatic media. HA strongly binds to clays and metal oxides [1–6], which affects the properties of these minerals significantly [7–9]. The interaction also affects the transport and reactivity of HA in natural systems [10]. The adsorption of HA may prevent HA from being washed away and decrease the rate of its decomposition, which is important for the conservation of soil organic matter and carbon sequestration [11,12]. To understand the fate of HA in soils, sediments and aquatic media, it is important to know the mechanisms/modes of the adsorption of HA on mineral surfaces.

Due to the heterogeneity of HA, complexity of its composition and conformation, and the differences in its interactions with different minerals, various adsorption mechanisms have been observed for HA-mineral interactions, such as ligand exchange, cation bridging, electrostatic attraction, H-bonding and hydrophobic interaction [2,3,13]. Although a number of studies have been performed on the adsorption of HA on minerals, it has not been well elucidated how differences mineral properties affect the adsorption mechanisms of HA.

Among minerals, clays (alumino-silicate minerals) hold a special position due to (i) the presence of basal and edge faces with different properties, and (ii) strong structural differences among different clays. Kaolinite and montmorillonite have distinct structural differences and are widely used in adsorption studies [14,15]. Kaolinite (1:1) is a clay composed of layers of one tetrahedral silica sheet (T) fused to one octahedral alumina sheet (O), whereas montmorillonite (2:1) is composed of layers of one octahedral (O) and two tetrahedral (T) sheets [16]. Both montmorillonite and kaolinite have negative sites on the basal faces owing to isomorphic substitution and amphoteric sites on the edge faces [16]. The amphoteric sites are conditionally charged and pH dependent because either a net positive or net negative charge can develop due to proton adsorption. Compared with montmorillonite, which has a high permanent layer charge, kaolinite has a low permanent charge and a significant variable charge [17]. These differences lead to different charging behaviors of the two clays [17,18]. A recent study on kaolinite has revealed that the O basal planes are also amphoteric with a clear variation of charge with pH and an isoelectric point between pH 6 and 8 [19].

The adsorption of humic substances on clay minerals is influenced by solution chemistry. In general, strong adsorption has been observed at low pH [20,21]. For example, ligand exchange and/or electrostatic interactions (attraction/repulsion) have been proved to be responsible for the pH dependence [2,13]. Adsorptions via ligand exchange and electrostatic attraction are believed to be dominant mechanisms for the binding of humic substances on the edges of clay minerals, especially at low pH [2]. Nonetheless, significant adsorption can still be observed under electrostatically unfavorable conditions. For instance, a maximum adsorption capacity of about 37% was observed for HA adsorption on kaolinite at pH 9.0 [22], which may be due to hydrophobic attraction [21] and/or hydrogen bonding. At high pH, some hydrophobic interaction may still occur although HA has both hydrophobic and hydrophilic parts and it becomes increasingly hydrophobic at low pH when the acidic groups are more protonated [23].

Further investigations are required to fully understand the mechanisms of HA adsorption on clay minerals. Thus, this study was aimed to investigate the effect of pH on the adsorption of HA on kaolinite and montmorillonite and to specify the contributions of various adsorption mechanisms. To this end, analytical techniques including adsorption measurements, isothermal titration calorimetry (ITC) and attenuated total reflectance Fourier transform infrared (ATR-FTIR) spectroscopy were combined to investigate the adsorption of HA on montmorillonite and kaolinite at different pH values. ATR-FTIR can provide information about the clay surface groups that play roles in the adsorption. ITC is a microcalorimetric technique to study chemical binding processes at a constant temperature [24,25] and enables the identification of the energetics associated with the adsorption process. By combining the adsorption isotherms results with the ITC results, the molar Gibbs energy of adsorption can be separated into enthalpy and entropy contribution, which provide further insights into the adsorption mechanisms of HA on the two clay minerals.

2. Materials and methods

2.1. Materials

2.1.1. Water and chemicals

Tap water was purified using an Aquapro water system (AJY-1001-U) to provide pure water with a resistivity of 18.45 MΩ cm. All reagents used were of analytical grade.

2.1.2. Humic acid

Soil HA was extracted from the upper horizon of meadow soil of Jiugong Mountain at an altitude of 1665 m in Hubei (N 29°27′, E 114°42′), China (Acid Udic Cambosols according to Chinese Soil Taxonomy [26]). The soil HA, which was denoted as JGHA, was isolated and purified according to the method of the International Humic Substances Society (IHSS) [27]. The sample in acid form was dialyzed for about three months until the pH reached 6.0, then freeze-dried and stored in a desiccator with silica gel. The weight average molar mass of JGHA determined by size exclusion chromatography was around 38 kDa. The elemental analysis (on an ash-free basis) showed 55.8% C, 38.9% O, 4.6% H, and 0.6% N (wet weight) [28]. The charge densities of JGHA in 0.1 mol/L KCl at pH 4.0, 6.0 and 8.0 were −0.9, −2.3 and −3.0 mmol/g, respectively [29].

A stock solution of 4.0 g/L JGHA in 0.1 mol/L KCl was prepared in a volumetric flask by dissolving JGHA under mild shaking for 24 h and at pH 10 to ensure full dissolution [30].

2.1.3. Clay minerals

Kaolinite (KGa-2) and montmorillonite (SWy-2) used in this study were purchased from the Clay Minerals Society Source Clays Repository (University of Colorado, USA) with purities of 95–100% and 90–100%, respectively. The cation exchange capacities (CECs) quoted by the supplier were 3.3 (KGa-2) and 76.4 meq/100 g (SWy-2). The samples were oxidized with H_2O_2 to remove any residual organic matter and the fractions < 2 μm were separated

by wet sedimentation. Then the fractions < 2 μm of montmorillonite (MON) and kaolinite (KAO) were washed five times with 0.1 mol/L KCl solution to bring the clays in K^+ form. To remove the excess KCl, the samples were washed with deionized water until no chloride could be detected by $AgNO_3$ solution. Then, the treated clays were freeze-dried and ground to pass through a 100-mesh sieve and stored. The specific surface areas of the dried and ground MON and KAO, obtained by N_2 gas adsorption and using the BET-method, were 19.7 m^2/g for KAO and 23.3 m^2/g for MON. The *t*-plot analysis using the standard N_2-isotherm equation of de Boer [31] revealed that the external surface area of MON sample was 16.3 m^2/g. The KAO sample was non-porous. More details of the gas adsorption analysis of MON and KAO were listed in the SI.

Stock suspensions of MON and KAO at pH 4.0, 6.0 and 8.0 in 0.1 mol/L KCl were prepared under continuous stirring (4.0 g/L for the adsorption isotherm measurements and ATR-FTIR analyses, and 8.0 g/L for the ITC titrations).

2.2. Methods

2.2.1. Adsorption isotherms

Adsorption isotherms at a given pH were obtained by batch experiments using the depletion from solution method. Before the experiment, the clay suspensions and JGHA solution were purged overnight with N_2 (g) to remove CO_2. Each batch sample was prepared by transferring to a 50 mL polypropylene centrifuge tube (1) an aliquot of the stock MON or KAO suspension and (2) an amount of JGHA stock solution. Then, the pH of the suspensions in the tubes was measured and adjusted to the target values (4.0, 6.0 and 8.0) by using 0.05 or 0.1 mol/L HCl or KOH when necessary. The final concentration of MON or KAO in the tubes was 1.0 g/L and that of JGHA ranged from 50 to 1400 mg/L and the total volume was 20 mL. The suspensions were equilibrated at 25 ± 1 °C by end-over-end rotation for 24 h. The pH was checked three to four times and readjusted to the target pH when necessary (the small volumes of acid or base required were measured and added to the total volume). Before pH checking the suspensions at pH 6.0 and 8.0 were kept under N_2 atmosphere for 10 min. After equilibration, the samples were centrifuged at 8000*g* for 15 min and the supernatants were filtered through a 0.45 μm nylon membrane filter. Each filtrate was analyzed for total organic carbon (TOC) with an Elementar TOC Select (Germany) apparatus. The JGHA concentrations were obtained from the TOC measurements by using a TOC-$JGHA_{conc}$ calibration line. The adsorption amounts of JGHA (mg/g) were calculated from the difference between the initial and final JGHA amounts in the solution and the mass of clay present. For the conversion of mg/g to μmol/g, we used the measured JGHA molar mass of 38 kDa.

2.2.2. ATR-FTIR spectroscopy

All ATR-FTIR spectra were recorded with a Bruker Vertex 70 spectrometer (Bruker Optics, Billerica, MA) using a MIRacle™ ATR accessory (Pike Technologies Spectroscopic Creativity, Madison, WI) equipped with a ZnSe ATR crystal at ambient temperature (25 ± 1 °C). The angle of incidence for the ATR cell was ~45°, which was far beyond the critical angle. The ATR-FTIR samples were pure clays and clay-JGHA complexes at pH 4.0, 6.0 and 8.0, and 0.1 mol/L KCl. The JGHA concentrations in the clay-JGHA complexes were matched to the maximum adsorption at the given pH. Each sample suspension (pure clay and clay-JGHA complex) was centrifuged (8000*g* for 15 min), and the supernatant was filtered and used for recording the background spectra prior to sample measurement. Before the collection of a background spectrum, the ATR crystal was carefully cleaned with ethanol to remove any residues of the previous sample. The subsequent sample measurements were carried out with small solid samples taken from the precipitate. At a randomly selected point of the precipitation with a fixed amount of precipitate (0.05 *g*) was removed with a small medicine spoon and mounted on a round ZnSe crystal to collect the spectrum with HgCdTe detector. This process was repeated two/three times for each sample and samples of equal weight were used. The spectra were obtained using standard spectral collection techniques and the rapid-scan software in OPUS 6.5. Each measured spectrum was based on 512 scans at 4 cm^{-1} in the range of 700–4000 cm^{-1}. The spectra were measured in duplicate/triplicate to verify the reproducibility of the results.

All sample spectra were background subtracted and baseline corrected with OPUS 6.5 software and then normalized by Origin 8.0 in order to make the band absorbance comparable among the samples. The spectra of MON and MON-JGHA complexes were normalized using the band area at 915 cm^{-1} and those of KAO and KAO-JGHA complexes were normalized by using the band area of the inner hydroxyl group band located at 3620 cm^{-1}.

The normalized ATR-FTIR spectra were further unraveled with Origin 8.0 using the second derivative method to approximate the peak positions, followed by deconvolution of the spectra in Gaussian bands [32]. The peak positions were further refined to obtain the best fit to the spectra and the band areas of the characteristic absorption bands were calculated. The deconvoluted spectra of the clay minerals and clay-JGHA complexes were shown in Figs. S2–S4. Thus, the obtained results were used to study the effects of changes in conditions: (1) the effect of pH on pure clay spectra, with the clay at pH 4.0 as reference and (2) at each pH, effect of adsorbed JGHA on KAO and MON with pure clay as reference. To quantify the spectral changes of band area ratios, *R*, were used, where *R* of a band was the sample normalized deconvoluted band area at a given wavenumber divided by the reference were used.

2.2.3. Isothermal titration calorimetry (ITC)

ITC experiments were performed using a TAM III (Thermometric AB, Sweden) micro-calorimeter equipped with a stainless steel titration ampoule (1 mL) and Hamilton syringe (250 μL) with a stainless steel needle (150 μm of inner diameter and 1.2 m of length). The calorimeter was positioned in a temperature-controlled environment (25.0 ± 0.1 °C) and calibrated by a standard electric pulse. Prior to each experiment, the sample cell and the syringe were rinsed with freshly distilled water. Solutions were thoroughly degassed prior to experiments to avoid air bubbles in the calorimeter. The clay suspension (0.4 mL, 8.0 g/L in 0.1 mol/L KCL equilibrated at the desired pH) was brought into the titration ampoule and stirred at 120 rev/min by a three-blade golden propeller. The ampoule was lowered into the calorimeter step by step, and allowed to equilibrate for at least 120 min before data collection. The needle of the syringe with JGHA stock solution (4.0 g/L in 0.1 mol/L KCl at the desired pH) was inserted through the sleeve on the titration unit till the needle tip submerged into the solution in ampoule. After a highly stable power value (W) was obtained (signal deviation < 200 nW in 5 min), the titration was started by the injection of aliquots of JGHA solution into the ampoule. A total volume of 120 μL JGHA solution was titrated into the ampoule in 12 injections of 10 μL at a rate of 1 μL/s. The time interval between two injections was 5 min. The baseline of the calorimeter did not change significantly within 5 min, and it thus was assumed that the adsorption reaction was equilibrated [33]. The calorimeter response of *power* (W) *vs. t* (min) was transformed with the calibration pulse (J/W) into a heat flow (J/min). The heat flow resulting from a sample titration included two contributions: the heat from the dilution of the stock clay suspension and stock JGHA solution upon the addition of JGHA solution, and the heat from the interaction between clay and JGHA. In an additional experiment, it was

verified that JGHA did not lead to the dissolution of the clays under the given conditions. The two heat flows of dilution were separately measured and subtracted from the heat flow measured for a sample titration. The remaining heat effect was regarded to be caused by "heat of adsorption" due to the adsorption of JGHA on the clay.

3. Results and discussion

3.1. Adsorption isotherm analysis

JGHA adsorption isotherms on KAO and MON at 0.1 mol/L KCl and three pH values are depicted in Fig. 1. All isotherms show a sharp rise at low JGHA (equilibrium) concentrations and then gradually level off at higher concentrations to a plateau value that is pH dependent. The shape of the isotherms can be classified as a high affinity type. The JGHA adsorption on both clays decreased with increasing pH, which is qualitatively in agreement with the results of previous studies [4,13]. At pH 4.0, similar maximum adsorptions (about 9.0 μmol/g) were observed for KAO and MON; but at pH 6.0 and 8.0, the maximum adsorption on MON (8.5 and 7.4 μmol/g, respectively) was significantly higher than that on KAO (5.5 and 4.5 μmol/g, respectively). Most likely only the external specific surface areas of the two clays are available for JGHA adsorption. By using these areas, the adsorption amounts can be expressed as μmol/m^2 (right side Y-axis of Fig. 1). It turned out that at three pH values, the adsorption amounts (μmol/m^2) were only slightly higher on MON than on KAO, indicating that both the external basal faces and edge faces contribute to the JGHA adsorption.

The isotherms could be well fitted to the Langmuir equation: $q = q_m K_L C^*/(1 + K_L C^*)$, where q is the amount of JGHA adsorbed per unit mass, q_m is the maximum amount of JGHA that can be adsorbed, C^* is the normalized equilibrium concentration based on a standard state of 1 mol/L, i.e., $C^*[-] = C$ (mol/L)/1 (mol/L) and K_L is the affinity constant (1 mol/L standard state). The fitting was carried out using Origin 8.0, and the obtained parameter values are presented in Table 1. The values of $\ln K_L$ can be converted to molar Gibbs energies of adsorption ΔG using the relation $-RT\ln K_L = \Delta G$. The calculated ΔG values are also shown in Table 1. The simple Langmuir equation fits the results well, indicating that the molar Gibbs energy of adsorption is not significantly affected by the adsorption amount in the measured adsorption window. For a given pH, the K_L values follow the order of *KAO* > *MON*, indicating that the molar Gibbs energy of JGHA adsorption (in absolute value) is higher for KAO than for MON.

The fact that pH strongly affects the adsorption indicates that electrostatic interactions play a significant role in JGHA adsorption on the two clays, especially for KAO. The permanent negative charges on the basal T-face of MON and KAO are pH independent [6,34] and are mainly compensated by specific adsorption of K^+ ions. Therefore, pH only has modest effects (K^+ exchange by H^+) on the state of the T-face. The pH variable charge on the small edge-face of MON and of KAO and on the basal O-face of KAO [19] is due to the reaction of O-containing surface sites with H^+ or OH^- in solution. This leads to positive ($AlOH_2^+$) or negative (AlO^- and SiO^-) surface charges depending on the pH, and this charge is largely compensated in the diffuse layer in the presence of KCl. The state of variable charge groups is therefore important for JGHA adsorption.

In general, the role of the pH on the adsorption of JGHA is twofold; both the JGHA interaction with the surface and the lateral interaction between the adsorbed JGHA particles are affected. As for the surface-JGHA interaction, increasing of pH leads to a decrease of the positive charge or an increase of the negative charge of the edge-face of the two clays as well as on the O-face of KAO. Thus, the electrostatic interaction of JGHA with the clay surface is also affected: with increasing pH, the attraction decreases or the electrostatic repulsion increases, which tends to decrease the JGHA adsorption for all JGHA concentrations. The effect is stronger for KAO than for MON because the edge area fraction of KAO is larger than that of MON [17] and the O-face of KAO also contributes to the effect [19]. The effects of pH and clay types on the surface-JGHA attraction are quantified by K_L values, which are higher for KAO than for MON at given pH and decrease with increasing pH for a given clay.

The second effect of pH is on the lateral interaction. Increasing of pH elevates the charge density of JGHA, which leads to increase of lateral electrostatic repulsion between the adsorbed JGHA particles and two types of surfaces. Moreover, the lateral repulsion becomes stronger with increasing JGHA adsorption and is therefore most relevant at high adsorption values. The plateau adsorption of JGHA and the fact that these plateaus decrease with increasing pH are therefore primarily due to the increasing lateral repulsion between adsorbed JGHA particles. It should be noted that the Langmuir equation does not account for lateral interactions. The measured effective affinity constant (K_L) of JGHA adsorption to quantify the JGHA-surface attraction by together with a *pseudo* maximum adsorption value (q_m) that is largely due to the lateral

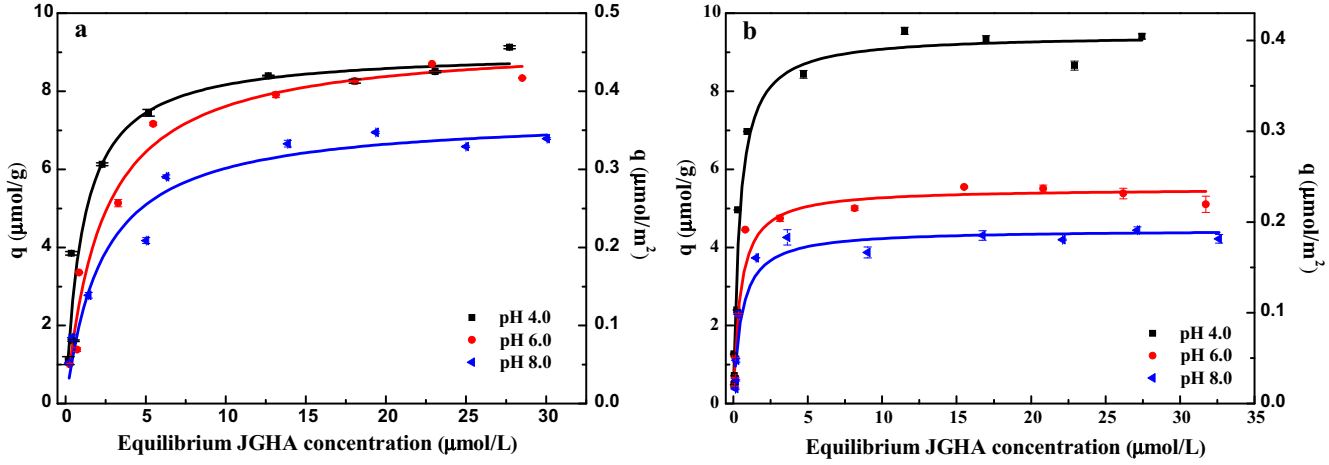

Fig. 1. Adsorption isotherms of JGHA on MON and KAO at 0.1 mol/L KCl and pH 4.0, 6.0 and 8.0; panel a: JGHA adsorption on MON, panel b: JGHA adsorption on KAO. Symbols: experimental results, the error bars indicate the standard deviation; solid lines: fitted Langmuir equation.

Table 1
Parameters of the Langmuir equation used to describe the JGHA adsorption on MON and KAO at three pH values.

	pH	q_m (μmol/g)	$K_L \times 10^6$	$\ln K_L$	ΔG (kJ/mol)	R^2
Montmorillonite						
	4.0	9.0 ± 0.5	0.98 ± 0.24	13.8	−34.2	0.95
JGHA	6.0	8.5 ± 0.4	0.44 ± 0.08	13.0	−32.2	0.97
	8.0	7.4 ± 0.4	0.24 ± 0.09	12.4	−30.7	0.92
Kaolinite						
	4.0	9.5 ± 0.3	2.42 ± 0.26	14.7	−36.4	0.97
JGHA	6.0	5.5 ± 0.2	2.19 ± 0.29	14.6	−36.2	0.96
	8.0	4.5 ± 0.2	0.89 ± 0.05	13.7	−33.9	0.94

q_m is maximum adsorption capacity, K_L is adsorption affinity constant and R^2 indicates the goodness of fit.

repulsion between JGHA and only partly due to surface saturation. The $\ln K_L$ value, or for that matter ΔG_L, therefore does not fully account for the interactions that govern the JGHA adsorption, the lateral repulsion is hidden in the q_m value.

The pH of zero net proton charge (pH_{ZNPC}) of the edge-face on MON is around 4.5 [17] and that on KAO is 6–7 [35] and the isoelectric point of O-face of KAO is 6–8 [19]. Thus, for the edges and the O-face of KAO, both the lateral and surface electrostatic interactions are repulsive at pH 8.0. Also, the T-face of the clays is negatively charged, but as this charge is largely compensated by specific adsorption of K^+ ions, the electrostatic repulsion between the T-face and JGHA is small. Therefore, the considerable adsorption at pH 8.0 is primarily due to adsorption on the T-face of KAO and MON, implying that besides electrostatic interaction, other interactions are important as well.

The significant HA adsorption on clays observed at alkaline pH has often been taken as an indirect evidence for hydrophobic interaction [36,37]. Also for JGHA this is plausible, because of the large amount of hydrophobic groups indicated by the relatively high carbon content of JGHA (55.8%). The clay edges are generally considered as quite hydrophilic, so the edge face hydrophobic interaction will not play a role. The two basal planes of MON are T-faces and these faces are basically hydrophobic, but the hydrophobicity is decreased by the negative charge density due to the isomorphic substitution [38,39]. KAO has only one partially hydrophobic basal plane (T-face), and the basal O-face is gibbsite-like with OH groups and is highly hydrophilic [40]. Based on these facts, the much higher adsorption of JGHA on the surface of MON than on KAO at pH 8.0 can be explained at least partly by hydrophobic interaction and, vice versa, hydrophobic interaction is important for JGHA adsorption on the T-faces. H-bonding is also a possible interaction mechanism next to hydrophobic attraction [41,42]. H-bonding can occur between the functional groups of JGHA and the partially hydrated and specifically adsorbed cations that compensate the isomorphic substitution charge of the T-face. At relatively high KCl concentration (0.1 mol/L), the state of T-face is hardly affected by pH, but the state of the JGHA functional groups is pH dependent. Therefore, it can be speculated that both H-bonding and the hydrophobic interaction are somewhat pH dependent.

3.2. Analysis of the ATR-FTIR spectra

The ATR-FTIR spectra of KAO and KAO-JGHA are depicted in Fig. 2 and those of MON and MON-JGHA in Fig. 3. Due to the low JGHA amounts present, the equipment could not detect the adsorption bands of JGHA. Therefore, the clay-JGHA spectra only show the bands of the two clays. To identify the absorption bands, the characteristic frequencies and their chemical identification as tabulated by Madejová and Komadel [43] were used (Table S1, SI).

In the 850–1150 cm^{-1} range, the spectra of pure KAO and MON show Si-O stretching and bending as well as OH bending absorptions (Figs. 2a and 3). The differences between KAO and MON (1:1 versus 2:1) are reflected by the shapes and positions of the bands. The band at about 913 cm^{-1} corresponds to the Al-OH deformation of inner hydroxyl groups and is present in the spectra of both clays. This inner hydroxyl group were used to normalize the spectra of MON. The band near 915 cm^{-1} of KAO is significantly larger than that of MON, which is related to the higher Al-OH content in KAO [44]. The OH bending band of KAO near 939 cm^{-1} arises from the vibrations of inner-surface OH groups, but this band is absent in the MON spectra. The two sharp absorption bands at 1005 and 1030 cm^{-1} of KAO are characteristic of in-plane Si-O stretching; as for MON, these Si-O stretching bands are shifted to 1023 and 1043 cm^{-1} and the bands are considerably overlapping. The bands near 1085 and 1115 cm^{-1} are assigned to Si-O stretching and are present in the spectra of both KAO and MON.

KAO, which has mostly Al in the octahedral positions, has four absorption bands in the OH stretching region from 3570 to 3730 cm^{-1} (Fig. 2b). The inner hydroxyl groups that link the T and O sheets give the absorption band near 3620 cm^{-1}. This OH group was used to normalize the KAO spectra. The strong band at 3693 cm^{-1} corresponds to the in-phase coupled vibration of perpendicular-interlayer-OH, whereas the bands at 3653 and 3674 cm^{-1} are due to out-of-phase coupled vibrations of these groups. These three interlayer groups are also exposed at the edge-face and the octahedral basal plate. In contrast to KAO spectra, the spectra of MON do not show clear OH stretching bands in the 3570–3730 cm^{-1} region.

To evaluate the pH sensitivity of the spectra of pure MON and KAO, the band areas of the deconvoluted spectra were calculated. When the peaks were close, it was difficult to resolve the individual bands unambiguously, and in such cases the areas of the bands that correspond to the same chemistry were added to obtain a total area. The characteristic bands and their peak frequencies are collected in Table 2, together with the calculated normalized areas and area ratios R. For each pure clay, the calculated ratios (R_1) indicate the band changes at the given pH relative to pH 4.0. For MON, the normalized areas of the combined Si-O bands near 1023 & 1043 cm^{-1} are slightly pH dependent, and at pH 6.0 the area is reduced by 5% and at pH 8.0 by 11% as compared with at pH 4.0. The total areas of the Si-O bands of KAO near 1005 & 1030 cm^{-1} show a similar tendency. R_1 is reduced by 21% at pH 6.0 and by 14% at pH 8.0. These results are in agreement with the fact that the Si-O bands of the basal planes are not affected by pH but some Si-O bands exposed at the edges are affected [43]. The area ratios of the combined bands of KAO near 913 & 939 cm^{-1} (Al-OH deformations) are decreased by about 20% from pH 4.0 to pH 6.0 or pH 8.0, indicating the presence of adsorption at the edges and O-face. The areas of OH bands near 3693 cm^{-1} at pH 6.0 and 8.0 fluctuate around that at pH 4.0. Clearly, those bands are insensitive to pH and thus may be attributed to basal plate groups.

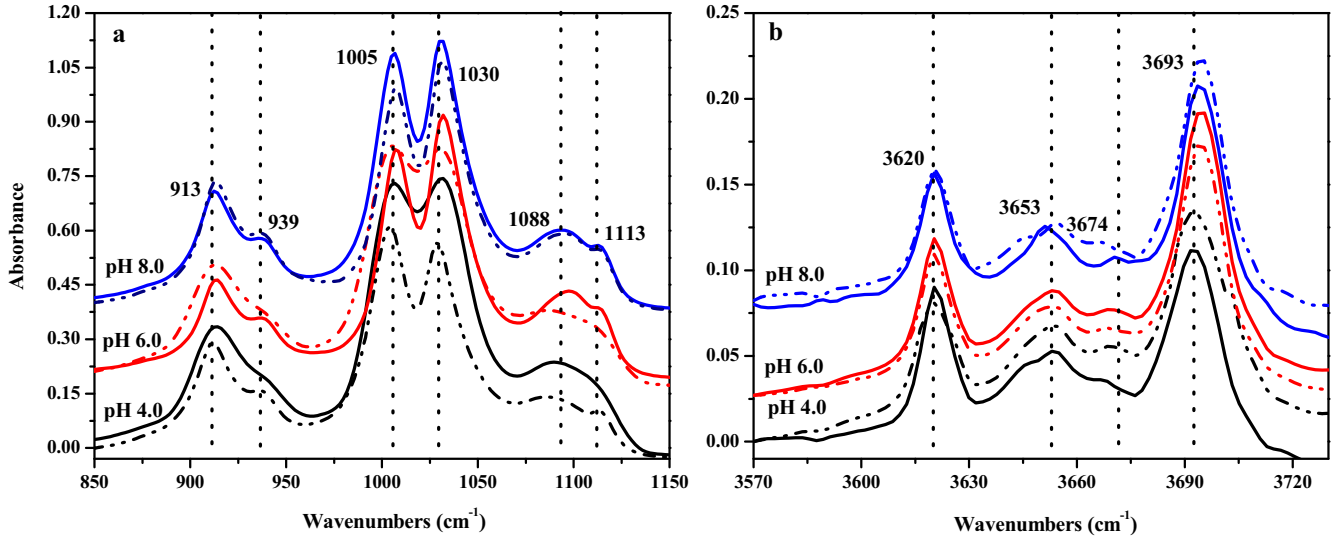

Fig. 2. ATR-FTIR spectra of KAO and KAO-JGHA complexes at pH 4.0, 6.0, and 8.0. Solid curves represent pure KAO and the dotted curves represent the KAO-JGHA complexes. Panel (a) depicts the absorbance values ranging from 850 to 1150 cm^{-1}, panel (b) those from 3570 to 3730 cm^{-1}.

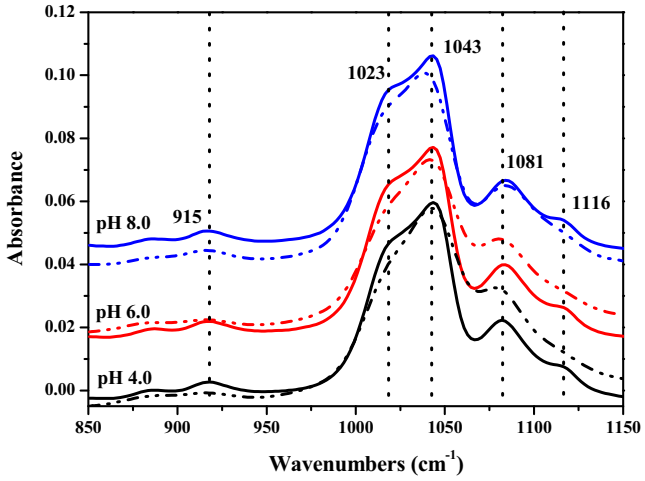

Fig. 3. ATR-FTIR spectra of MON and MON-JGHA complexes at pH 4.0, 6.0 and 8.0; the absorbance values range from 850 to 1150 cm^{-1}. Solid curves represent pure MON samples and the dotted curves stand for MON-JGHA complexes.

The effect of JGHA adsorption was investigated in a similar way by comparing the summed normalized band areas of the deconvoluted bands in the absence and presence of JGHA. At given pH, the area ratios R_2 represent the effect of adsorbed JGHA on the band areas. In general, the band areas of groups are affected by JGHA include Si-O bands of MON and KAO and OH stretching of inner-surface hydroxyl groups on the surface of KAO, and the ratios become smaller due to JGHA adsorption ($R_2 < 1.0$). These results imply a strong attraction between these groups and JGHA groups. The ratios R_2 of the Si-O bands at 1081 & 1116 cm^{-1} of MON (0.67–1.09) and at 1088 & 1113 cm^{-1} and 3653 & 3674 cm^{-1} of KAO (0.36–1.04) increase with increasing pH, which is consistent with the decreasing adsorption with increasing pH (Fig. 1). For KAO, the R_2 values of these bands indicate that the main difference is between pH 4.0 and pH 6.0 (1088 & 1116 cm^{-1}: 0.36–0.88; 3653 & 3674 cm^{-1}: 0.50–0.94). As for MON, the increase of R_2 is gradual. Based on the fact that all bands are affected by the presence of JGHA, it may be concluded again that both the edge and basal faces contribute to JGHA adsorption.

The decrease in band areas of hydroxyl groups on the surface of KAO near 3653 & 3674 cm^{-1} most likely implies the formation of surface complexes at the edge and O-face via ligand exchange. Arnarson and Keil [13], Zhang *et al.* [21] and Parfitt *et al.* [45] have spectroscopically proven that ligand exchange (carboxyl and hydroxyl groups of humic substances versus surface hydroxyl groups of clay minerals) is a major mechanism for HA adsorption on clays. Ligand exchange is affected by the charged state of the surface groups and thus by pH. The ligand exchange is also partly responsible for the adsorption of JGHA on MON, but the edge OH groups of MON could not be detected due to the small edge surface. It can be concluded that the contribution of ligand exchange to JGHA adsorption is larger for KAO than for MON.

3.3. ITC results and thermodynamic analysis of JGHA adsorption

The calorimeter responses of the JGHA titrations of MON and KAO suspensions are depicted in Fig. 4 (*Power* in μW *vs. t* in min). The positive peaks reflect exothermic heats of adsorption. After transformation to mJ/min with the calibration pulse and correction for the heats of dissolution, heats of adsorption (mJ/min) were calculated, and by integrating the area under the peaks, the heat of adsorption per JGHA addition (Q in mJ/g) was obtained.

Using the measured adsorption isotherms, the total JGHA addition (μmol/g) at time t can be separated into adsorbed JGHA (μmol/g) and JGHA in solution (μmol/g). The cumulative heat of adsorption, ΣQ (mJ/g), can then be plotted *vs.* the adsorbed amount of JGHA (μmol/g). The results are depicted in Fig. 5 (solid symbols, panels at the top) for both MON and KAO. By comparing the X-axis of Fig. 5 with the adsorption values in Fig. 1, it can be seen from the ITC results that adsorption values are from low to modest. The comparison of the plots for MON and KAO reveals that released heat of adsorption on MON is larger than that on KAO at all three pH values. The slope of a ΣQ curve provides the molar enthalpy of adsorption ΔH (kJ/mol), and a constant slope for a range of adsorption values implies constant ΔH. By way of example, in the plots of MON and KAO at pH 4.0, two linear regions indicated that approximate the ΣQ curve reasonably well. The same can be done for the other pH values. Before continuing this line of reasoning, it is instructive to calculate discrete values of ΔH. This can be done by taking for each measured point the ratio $\Delta\Sigma Q$ (mJ/g)/Δads (μmol/g), and the results are depicted in the lower panels of Fig. 5

Table 2
Characteristics and peaks area of the bands of the ATR-FTIR spectra of the pure clays and the clay-JGHA complexes.

pH	Bands	Peak (cm^{-1})	$Area_1$	R_1[a]	Peak (cm^{-1})	$Area_2$	R_2[b]
	MON				*MON-JGHA*		
	OH	915	0.10	1.00	915	0.10	1.00
4.0	Si-O	1023 & 1043	2.77	1.00	1023 & 1044	1.38	0.50
	Si-O	1081 & 1116	1.28	1.00	1081 & 1116	0.86	0.67
	OH	915	0.10	1.00	915	0.10	1.00
6.0	Si-O	1022 & 1044	2.62	0.95	1022 & 1044	1.72	0.66
	Si-O	1082 & 1116	1.37	1.07	1082 & 1116	1.21	0.88
	OH	914	0.10	1.00	915	0.10	1.00
8.0	Si-O	1021 & 1045	2.33	0.89	1022 & 1043	1.91	0.82
	Si-O	1084 & 1116	1.04	0.76	1081 & 1116	1.13	1.09
	KAO				*KAO-JGHA*		
	Inner OH	3620	0.70	1.00	3620	0.70	1.00
	OH	913 & 939	17.23	1.00	912 & 938	8.66	0.50
	Si-O	1005 & 1030	38.46	1.00	1003 & 1030	23.83	0.62
4.0	Si-O	1088 & 1113	13.60	1.00	1088 & 1113	4.94	0.36
	OH	3653 & 3674	2.14	1.00	3653 & 3672	1.07	0.50
	OH	3693	1.85	1.00	3693	1.78	0.96
	Inner OH	3620	0.70	1.00	3620	0.70	1.00
	OH	913 & 939	13.86	0.80	913 & 940	12.72	0.92
	Si-O	1006 & 1030	30.29	0.79	1007 & 1031	27.20	0.90
6.0	Si-O	1090 & 1113	11.51	0.85	1088 & 1113	10.16	0.88
	OH	3652 & 3674	1.74	0.81	3653 & 3674	1.64	0.94
	OH	3695	2.05	1.11	3695	1.92	0.94
	Inner OH	3620	0.70	1.00	3620	0.70	1.00
	OH	913 & 939	13.46	0.78	914 & 940	11.35	0.84
	Si-O	1006 & 1030	32.91	0.86	1007 & 1030	28.85	0.88
8.0	Si-O	1090 & 1113	10.67	0.78	1091 & 1113	11.14	1.04
	OH	3650 & 3674	1.59	0.74	3651 & 3674	1.38	0.87
	OH	3694	1.74	0.94	3695	1.84	1.06

[a] R_1 is the ratio of the band area at the indicated pH with respect to the band area at pH 4.0 for pure clays.
[b] R_2 is ratio of band area of a clay-JGHA complex with respect to the band area of the pure clay at same pH condition.

(open symbols). From these figures, it can be seen that ΔH decreases dramatically with increasing adsorption of JGHA up to about 0.71, 0.62 and 0.48 μmol/g for MON and about 1.0, 0.87 and 0.74 μmol/g for KAO at pH 4.0, 6.0 and 8.0, respectively. For higher adsorbed amounts, the molar heats decrease only slightly. Both analyses point to two main regions for ΔH, but especially in region-1, the exothermic value of ΔH decreases with increasing adsorption. For both MON and KAO, initially preferential adsorption of JGHA occurs at the sites with high molar enthalpies and that at higher adsorption values, the sites with a lower and about constant molar enthalpy of adsorption become occupied.

Even in region-1, the experimental points of the ΣQ curves do not deviate much from a straight line. This indicates that the enthalpy of JGHA adsorption in region-1 can be described to a reasonably good approximation by an average ΔH in this region. The enthalpy-wise JGHA adsorption can then be described in the measured adsorption window as adsorption to two roughly homogeneous site types: site type 1 with a relatively high average molar enthalpy (region-1) and site type 2 with a relatively low average molar enthalpy (region-2). The average ΔH values of the two site types can be obtained from the slopes of the straight lines covering region-1 and region-2 of the ΣQ curves for the two clays at three pH values. The results are collected in Table 3. The adsorption at the intersection point of the curves approximately corresponds with the maximum adsorption on site type 1. This value is also included in Table 3.

The following observations can be made by comparing the results of MON and KAO. (1) At a given pH and adsorbed amount, the ΔH values of MON-JGHA are higher than those of KAO-JGHA. (2) Region-1 covers a larger adsorption range for KAO (roughly 1.0 μmol/g) than for MON (roughly 0.7 μmol/g). (3) In region-2, ΔH is closer to being constant for MON than for KAO. These differences are most likely due to the different structures of MON and KAO, since MON has two equal basal-faces (T) and a relatively small edge-face and KAO has two different basal-faces (T and O) and an edge-face with an area similar to that of the basal faces [17,46]. The more complex surface of KAO than of MON leads to stronger site heterogeneity of KAO.

For the calculation of ΔS, the molar entropy of adsorption, on the basis of the obtained values ΔG (adsorption isotherms) and ΔH (calorimetry) the relation: $\Delta G = \Delta H - T\Delta S$ applies. It should be noted that the lowest adsorption values measured with the isotherms (Fig. 1) are close to the adsorbed amount at the end of region-1, implying that for the thermodynamic analysis the isotherms have to be extrapolated to lower adsorption values. The adsorption isotherms could be fitted well to the Langmuir equation (Fig. 1 and Table 1); therefore, it can be also assumed that at adsorption values lower than the measured values, the adsorption can be described with the fitted Langmuir equation. The measured isotherms then indicated that K_L, and hence ΔG, are independent of the adsorbed amount at the given pH. The heterogeneity observed for ΔH (region-1 and region-2) is thus not reflected in ΔG but only in ΔS. The calculated values of $T\Delta S$ for region-1 and region-2 are also collected in Table 3. For site type 2, a maximum adsorption with the ITC measurements is also indicated. The larger exothermic ΔH values in region-1 than region-2 are reflected in the more negative values of $T\Delta S$ for region-1 than in region-2.

The high average exothermic enthalpy and large average entropy loss in region-1 indicate that the JGHA segments are strongly bound to the surface sites by enthalpic attraction and exclude hydrophobic attraction. In view of the small adsorbed amounts, this is most likely due to the strong heterogeneity of JGHA and the reaction of specific functional groups of JGHA with clay surface groups leading inner-sphere complexes. The decrease

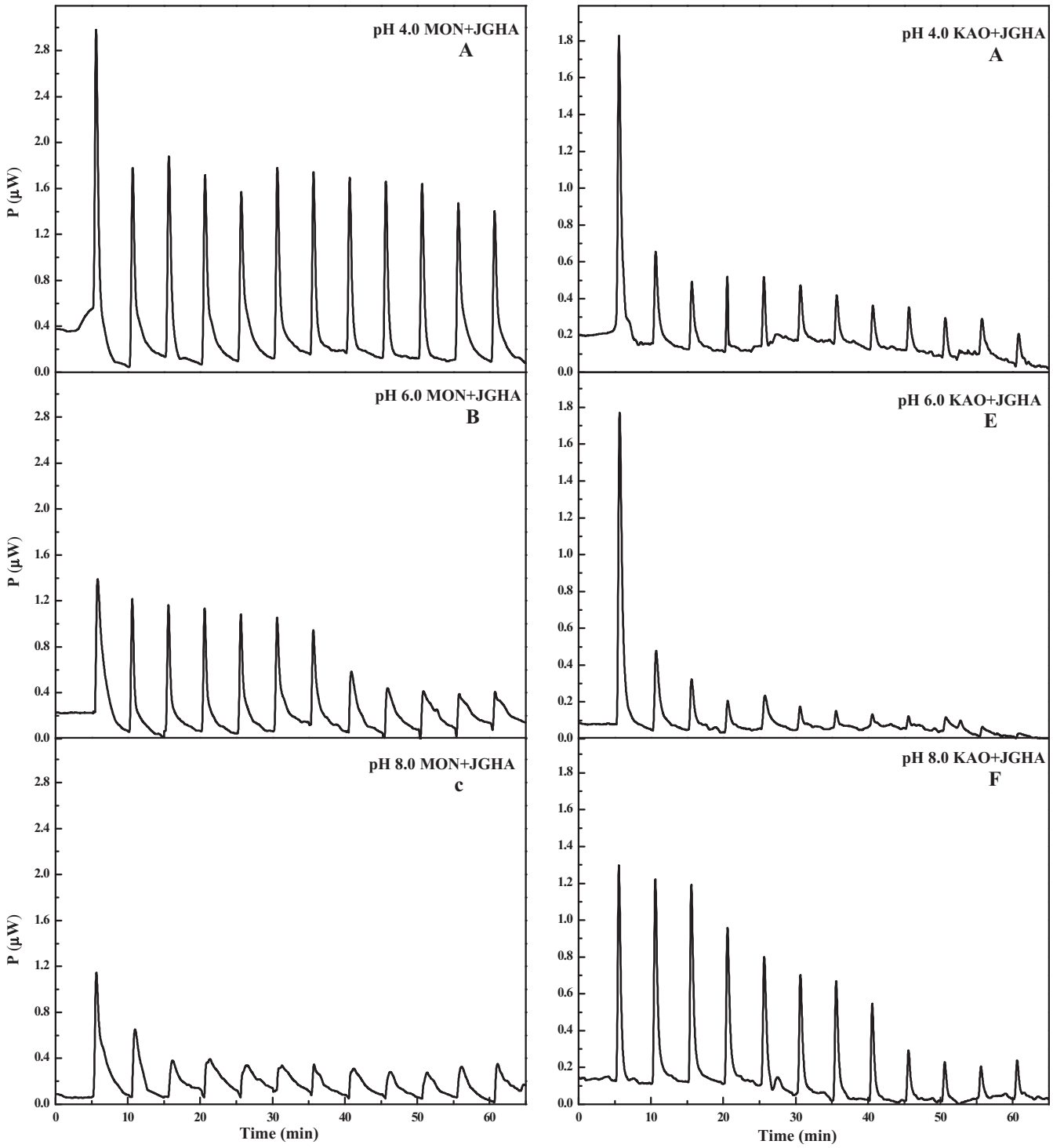

Fig. 4. Thermograms (power P *vs.* time) of titrations of JGHA (4 g/L, 0.1 mol/L KCl) into MON and KAO suspensions (8 g/L, 0.1 mol/L KCl). Panels A, B, C: JGHA titrated into MON suspensions at pH 4.0, 6.0 and 8.0, respectively. Panels D, E, F: JGHA titrated into KAO suspension at pH 4.0, 6.0 and 8.0, respectively.

of the exothermic ΔH with increasing pH (and no clear trend in $T\Delta S$) indicates that the variable charge groups of the clay surface are involved in the binding. Therefore, ligand exchange and electrostatic binding are the main adsorption mechanisms in region-1, which were emphasized before in [2].

In region-2, the behavior is more homogeneous (ΔG and ΔH are constant at the given pH) and also the pH effects on ΔH and $T\Delta S$ are more random. The average molar entropy loss in this region is lower than in region-1, which is likely due to the presence of hydrophobic binding next to surface complexation and electrostatic binding. The molar entropy of hydrophobic attraction is positive and this lowers the overall entropy loss. This indicates that in region-2, adsorption on the basal faces is also important. On the basal plates, H-bonding via specifically adsorbed hydrated cations might also be important (as concluded in Section 3.1). These results observed for region-1 and region-2 are consistent with the conclusion of a previous study [47] that strong adsorption sites exist at the edges of KAO and weak sites at the basal plates.

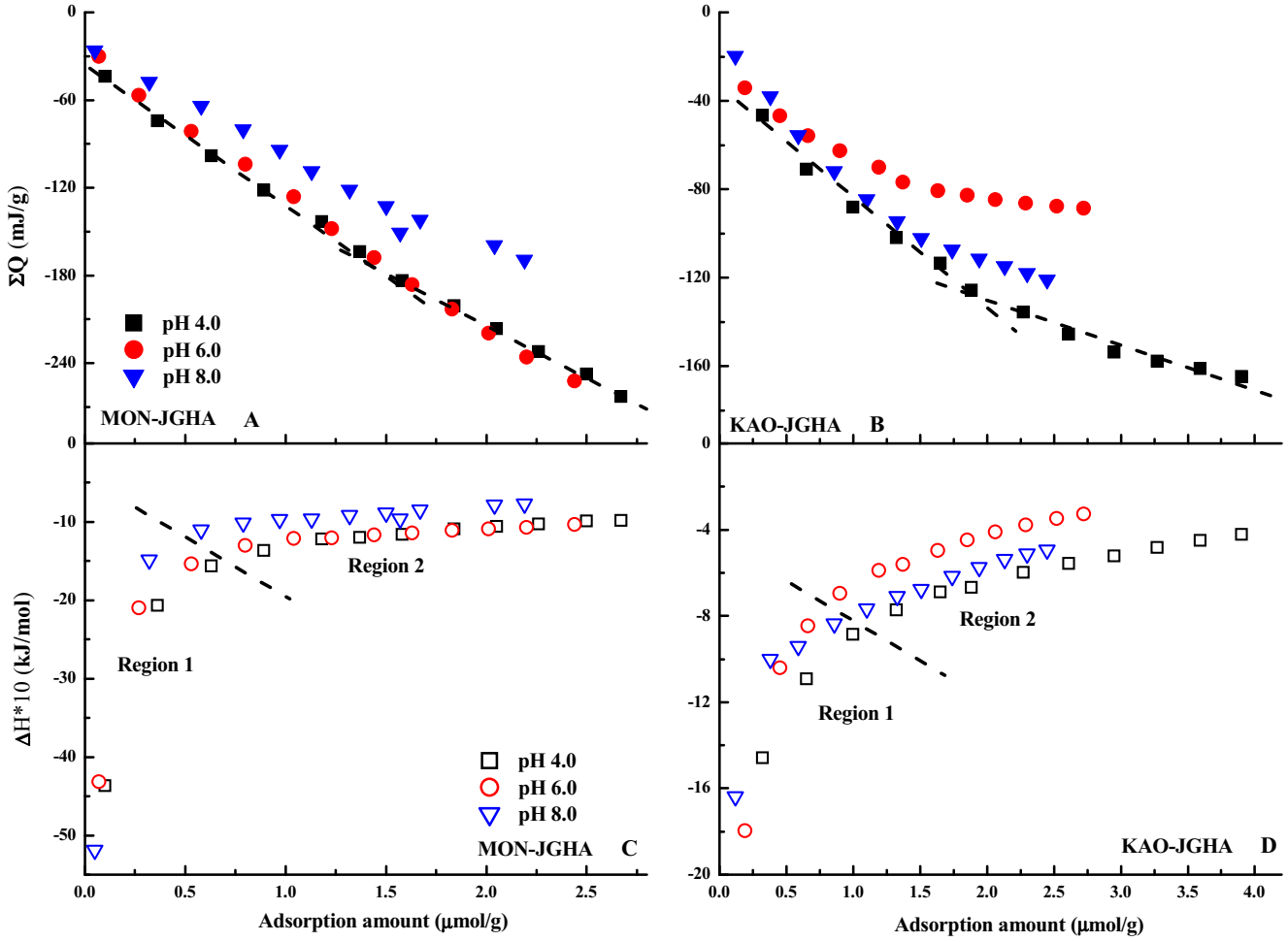

Fig. 5. Cumulative heat of adsorption of JGHA per g on clay (Σ*Q* in mJ/g; closed symbols) (panel A: MON-JGHA; panel B: KAO-JGHA) and the molar enthalpy (Δ*H* in kJ/mol; open symbols) of adsorption of JGHA on MON (panel C) or KAO (panel D), as a function of the adsorbed amount (μmol/g) at three indicated pH values.

Table 3
Thermodynamic parameters of JGHA adsorption on MON and KAO at T = 25 °C.

Receptors	pH	Site types	Ads_{max}	$\ln K_L$	Δ*H* (kJ/mol)	Δ*G* (kJ/mol)	TΔ*S* (kJ/mol)
	4.0	Site I	0.70	12.7	−136.6	−31.6	−105.0
		Site II	2.68	13.6	−98.4	−33.9	−64.5
MON	6.0	Site I	0.63	12.7	−125.1	−31.2	−93.9
		Site II	2.45	13.1	−103.4	−32.6	−70.8
	8.0	Site I	0.48	12.4	−97.0	−30.8	−66.2
		Site II	2.19	12.9	−77.3	−31.9	−45.4
	4.0	Site I	1.01	12.9	−88.5	−32.0	−56.5
		Site II	3.90	13.8	−42.3	−34.4	−7.9
KAO	6.0	Site I	0.89	12.9	−69.4	−31.9	−37.5
		Site II	2.72	13.4	−32.6	−33.0	0.4
	8.0	Site I	0.78	12.4	−76.8	−31.1	−45.7
		Site II	2.47	14.3	−49.3	−35.5	−13.8

The (average) molar enthalpies, Δ*H*, are determined by ITC, the molar Gibbs energies, Δ*G*, are derived from the adsorption isotherms using the Langmuir model and *T*Δ*S* is obtained using $\Delta G = \Delta H - T\Delta S$.
Ads_{max} represents the maximum adsorption amount of region-1 and region-2 corresponds to Fig. 5.

Based on the maximum adsorption amounts at the end of region-1 (mainly on variable charge edge sites) and region-2 (total adsorption on edge sites and basal planes) (Table 3), the contribution of the edge-face (ligand exchange and electrostatic attraction) to the total adsorption was calculated, and the estimated contribution is 26–32% for KAO and 22–26% for MON. These results are somewhat similar to those of Feng *et al.* [2], who reported that ligand exchange accounted for 32% of peat humic acid adsorption on montmorillonite and kaolinite. However, the estimated contribution of mechanisms only apply to the maximum adsorption of region-2.

At high adsorption values, when the lateral interactions become important, no experimental Δ*H* values are available. Moreover, as discussed above, the lateral interaction is not included in Δ*G*, but rather in the values of the plateau adsorption. Therefore, it is not feasible to extrapolate the thermodynamic parameters Δ*H* and

ΔS due to adsorption values higher than those indicated for region-2.

4. Conclusions

The adsorption of JGHA on KAO and MON occurs at the external surface of the clays and the adsorption decreases with increasing pH. The effect of pH is stronger for KAO than for MON. The pH dependent plateau values of the isotherms are largely due to lateral electrostatic repulsion. The isotherms at given pH can be described with a simple Langmuir equation, indicating that the affinity constant and hence the molar Gibbs energy of adsorption is independent of the adsorbed amount. However, the lateral electrostatic repulsion leads to the plateau values of the adsorption is not included in the (apparent) affinity by fitting the Langmuir equation to the measured isotherms, but in the maximum adsorption value.

Detailed analysis of the adsorption and ATR-FTIR results indicates that the adsorption on the edges of both clays as well as that at the O-basal plane of KAO are largely due to ligand exchange and electrostatic attraction. The pH dependence of JGHA adsorption plateaus for both clays is largely due to lateral electrostatic repulsion between the adsorbed JGHA particles. The JGHA adsorption on the T-basal faces is likely due to a combination of H-bonding and hydrophobic interaction.

At low adsorption amounts, a relatively high (heterogeneous) exothermic molar enthalpy and a relatively high negative molar entropy of adsorption are observed both for MON and KAO, which supports the binding of specific JGHA groups and the variable charge surface sites by ligand exchange and electrostatic attraction in the form of inner-sphere complexes. At moderate adsorption values, the molar enthalpy (negative) and entropy (negative) are smaller and not systematically dependent on pH, indicating that the basal T-planes are also involved in the adsorption. For KAO (1:1, different basal faces), the enthalpic heterogeneity in this region is larger than that of MON (2:1, same basal faces). The lower negative molar entropy might be due to a combination of ligand exchange plus H-bonding (entropy losses) and hydrophobic attraction (entropy gain).

The quantification of the contributions of different adsorption processes of soil HA on clay minerals improves our understanding on the formation of organic-inorganic nanocomposites. The results suggest that soils with different types of clays may be different in soil carbon pools and retention ability of organic contaminants.

Acknowledgments

This investigation supported by National Natural Science Foundation of China (Nos. 41330852 and 41425006) and the National Key Basic Research Program of China (No. 2015CB150504). We also like to thank Prof. Willem Norde for his help and advice with the isothermal titration calorimetry.

Appendix A. Supplementary material

Supplementary data associated with this article can be found, in the online version, at http://dx.doi.org/10.1016/j.jcis.2017.05.078.

References

[1] N. Kloster, M. Avena, Interaction of humic acids with soil minerals: adsorption and surface aggregation induced by Ca^{2+}, Environ. Chem. 12 (4) (2015) 37–39.
[2] X. Feng, A.J. Simpson, M.J. Simpson, Chemical and mineralogical controls on humic acid sorption to clay mineral surfaces, Org. Geochem. 36 (11) (2005) 1553–1566.
[3] E. Tombácz, Z. Libor, E. Illés, A. Majzik, E. Klumpp, The role of reactive surface sites and complexation by humic acids in the interaction of clay mineral and iron oxide particles, Org. Geochem. 35 (3) (2004) 257–267.
[4] J. Hur, M.A. Schlautman, Molecular weight fractionation of humic substances by adsorption onto minerals, J. Colloid Interf. Sci. 264 (2) (2003) 313–321.
[5] B. Gu, J. Schmitt, Z. Chen, L. Liang, J.F. McCarthy, Adsorption and desorption of natural organic matter on iron oxide: mechanisms and models, Environ. Sci. Technol. 28 (1) (1994) 38–46.
[6] E. Tombácz, A. Dobos, M. Szekeres, H.D. Narres, E. Klumpp, I. Dekany, Effect of pH and ionic strength on the interaction of humic acid with aluminium oxide, Colloid Polym. Sci. 278 (2000) 337–345.
[7] E. Illés, E. Tombácz, The effect of humic acid adsorption on pH-dependent surface charging and aggregation of magnetite nanoparticles, J. Colloid Interf. Sci. 295 (1) (2006) 115–123.
[8] E.M. Murphy, J.M. Zachara, S.C. Smith, Influence of mineral-bound humic substances on the sorption of hydrophobic organic compounds, Environ. Sci. Technol. 24 (10) (1990) 1507–1516.
[9] E. Tombácz, M. Szekeres, L. Baranyi, E. Michéli, Surface modification of clay minerals by organic polyions, Colloid Surface A 141 (3) (1998) 379–384.
[10] G.U. Balcke, N.A. Kulikova, S. Hesse, F.-D. Kopinke, I.V. Perminova, F.F. H., Adsorption of Humic Substances onto Kaolin Clay Related to Their Structural Features, Soil Sci. Soc. Am. J. 66 (6) (2002) 1805–1812.
[11] C. Chenu, Y.L. Bissonnais, D. Arrouays, Organic Matter Influence on Clay Wettability and Soil Aggregate Stability, Soil Sci. Soc. Am. J. 64 (2000) 1479–1486.
[12] C.R. Evanko, D.A. Dzombak, Influence of structural features on sorption of NOM-analogue organic acids to goethite, Environ. Sci. Technol. 32 (19) (1998) 2846–2855.
[13] T.S. Arnarson, R.G. Keil, Mechanisms of pore water organic matter adsorption to montmorillonite, Mar. Chem. 71 (3) (2000) 309–320.
[14] J. Baham, G. Sposito, Adsorption of dissolved organic carbon extracted from sewage sludge on montmorillonite and kaolinite in the presence of metal ions, J. Environ. Qual. 23 (1) (1994) 147–153.
[15] K. Wang, B. Xing, Structural and sorption characteristics of adsorbed humic acid on clay minerals, J. Environ. Qual. 34 (1) (2005) 342–349.
[16] H. Van Olphen, An Introduction to Clay Colloid Chemistry, Interscience Publisher, New York, 1963.
[17] E. Tombácz, M. Szekeres, Surface charge heterogeneity of kaolinite in aqueous suspension in comparison with montmorillonite, Appl. Clay Sci. 34 (1–4) (2006) 105–124.
[18] Y. Tsujimoto, C. Chassagne, Y. Adachi, Comparison between the electrokinetic properties of kaolinite and montmorillonite suspensions at different volume fractions, J. Colloid Interf. Sci. 407 (2013) 109–115.
[19] V. Gupta, J.D. Miller, Surface force measurements at the basal planes of ordered kaolinite particles, J. Colloid Interf. Sci. 344 (2) (2010) 362–371.
[20] J. Hur, M.A. Schlautman, Effects of pH and phosphate on the adsorptive fractionation of purified Aldrich humic acid on kaolinite and hematite, J. Colloid Interf. Sci. 277 (2) (2004) 264–270.
[21] L.C. Zhang, L. Luo, S. Zhang, Integrated investigations on the adsorption mechanisms of fulvic and humic acids on three clay minerals, Colloid Suface A 406 (2012) 84–90.
[22] R. Kretzschmar, H. Sticher, D. Hesterberg, Effects of adsorbed humic acid on surface charge and flocculation of kaolinite, Soil Sci. Soc. Am. J. 61 (1) (1997) 101–108.
[23] R.P. Schwarzenbach, P.M. Gschwend, D.M. Imboden, Environmental organic chemistry, John Wiley & Sons, 2005.
[24] D. Gorman-Lewis, J.B. Fein, M.P. Jensen, Enthalpies and entropies of proton and cadmium adsorption onto Bacillus subtilis bacterial cells from calorimetric measurements, Geochim. Cosmochim. Ac. 70 (19) (2006) 4862–4873.
[25] W.F. Tan, L.K. Koopal, W. Norde, Interaction between humic acid and lysozyme, studied by dynamic light scattering and isothermal titration calorimetry, Environ. Sci. Technol. 43 (3) (2008) 591–596.
[26] Z. Gong, G. Zhang, Z. Chen, Pedogenesis and soil taxonomy (Chinese), Beijing Sci. Press Publ., Beijing, 2007.
[27] R.S. Swift, Organic matter characterization, Methods of Soil Analysis Part 3—Chemical Methods (methodsofsoilan3) (1996) 1011–1069.
[28] Y. Li, W.F. Tan, L.K. Koopal, M.X. Wang, F. Liu, W. Norde, Influence of soil humic and fulvic acid on the activity and stability of lysozyme and urease, Environ. Sci. Technol. 47 (10) (2013) 5050–5056.
[29] W.F. Tan, J. Xiong, Y. Li, M.X. Wang, L.P. Weng, L.K. Koopal, Proton binding to soil humic and fulvic acids: experiments and NICA-Donnan modeling, Colloid Suface A 436 (2013) 1152–1158.
[30] M. Brigante, G. Zanini, M. Avena, On the dissolution kinetics of humic acid particles, Colloid Suface A 294 (1–3) (2007) 64–70.
[31] J.H.D. Boer, B.C. Lippens, B.G. Linsen, J.C.P. Broekhoff, A.V.D. Heuvel, T.J. Osinga, The t-curve of multimolecular N_2-adsorption, J. Colloid Interf. Sci. 21 (4) (1966) 405–414.
[32] K.G. Bhattacharyya, S. SenGupta, G.K. Sarma, Interactions of the dye Rhodamine B with kaolinite and montmorillonite in water, Appl. Clay. Sci. 99 (2014) 7–17.
[33] M.J. Avena, L.K. Koopal, Kinetics of humic acid adsorption at solid-water interfaces, Environ. Sci. Technol. 33 (16) (1999) 2739–2744.
[34] G. Sposito, R.J. Reginato, R. Luxmoore, Opportunities in basic soil science research, Soil Sci. Soc. Am. J. (1992).
[35] D.J.A. Williams, K.P. Williams, Electrophoresis and zeta potential of kaolinite, J. Colloid Interf. Sci. 65 (1) (1978) 79–87.

[36] M.A. Schlautman, J.J. Morgan, Effects of aqueous chemistry on the binding of polycyclic aromatic hydrocarbons by dissolved humic materials, Environ. Sci. Technol. 27 (5) (1993) 961–969.
[37] B. Gu, J. Schmltt, Z. Chen, L. Liang, J.F. McCarthy, Adsorption and desorption of natural organic matter on iron oxide: mechanisms and models, Environ. Sci. Technol. 28 (1994) 38–46.
[38] P. Kampeerapappun, D. Aht-ong, D. Pentrakoon, K. Srikulkit, Preparation of cassava starch/montmorillonite composite film, Carbohyd. Polym. 67 (2) (2007) 155–163.
[39] J.M. Douillard, J. Zajac, H. Malandrini, F. Clauss, Contact angle and film pressure: study of a talc surface, J. Colloid Interf. Sci. 255 (2) (2002) 341–351.
[40] M. Żbik, R.G. Horn, Hydrophobic attraction may contribute to aqueous flocculation of clays, Colloid Suface A 222 (1–3) (2003) 323–328.
[41] K.S. Katti, D.R. Katti, Relationship of swelling and swelling pressure on silica–water interactions in montmorillonite, Langmuir 22 (2) (2006) 532–537.
[42] S. Yeasmin, B. Singh, R.S. Kookana, M. Farrell, D.L. Sparks, C.T. Johnston, Influence of mineral characteristics on the retention of low molecular weight organic compounds: a batch sorption-desorption and ATR-FTIR study, J. Colloid Interface Sci. 432 (2014) 246–257.
[43] J. Madejová, P. Komadel, Baseline studies of the clay minerals society source clays: infrared methods, Clay. Clay. Miner. 49 (5) (2001) 410–432.
[44] J. Madejová, FTIR techniques in clay mineral studies, Vib. Spectrosc. 31 (1) (2003) 1–10.
[45] R.L. Parfitt, A.R. Fraser, V.C. Farmer, Adsorption on hydrous oxides. III. Fulvic acid and humic acid on goethite, gibbsite and imogolite, J. Soil Sci. 28 (2) (1977) 289–296.
[46] E. Tombácz, M. Szekeres, L. Baranyi, E. Micheli, Surface modification of clay minerals by organic polyions, Colloid Suface A 141 (3) (1998) 379–384.
[47] D.A. Sverjensky, N. Sahai, Theoretical prediction of single-site surface-protonation equilibrium constants for oxides and silicates in water, Geochim. Cosmochim. Ac. 60 (20) (1996) 3773–3797.